preprint, finally published in Flow, Turbulence and Combustion **71** *(2003), 5–17*

Control of Flow Separation Using Electromagnetic Forces

Tom Weier (t.weier@fz-rossendorf.de), Gunter Gerbeth (g.gerbeth@fz-rossendorf.de) and Gerd Mutschke (g.mutschke@fz-rossendorf.de)
Forschungszentrum Rossendorf, P.O.Box 51 01 19, D–01314 Dresden, Germany

Olgerts Lielausis (mbroka@tesla.lv)
Institute of Physics, University of Latvia, Salaspils 1, LV-2169, Latvia

Gerd Lammers (lammers@hsva.de)
Hamburg Ship Model Basin, Bramfelder Str. 164, D–22305 Hamburg, Germany

Abstract. If a fluid is electrically conductive, its flow may be controlled using electromagnetic forces. Meanwhile, this technique is a recognized tool even on an industrial scale for handling highly conductive materials like liquid metals. However, also fluids of low electrical conductivity as considered in the present study, like sea–water and other electrolytes, permit electromagnetic flow control. Experimental results on the prevention of flow separation by means of a streamwise, wall parallel Lorentz force acting on the suction side of inclined flat plates and hydrofoils will be presented.

Keywords: flow separation, flow control, Lorentz force

1. Introduction

Separation is an undesired flow feature in many engineering cases. Usually it implies a loss of lift, an increase of drag, diminished pressure recovery etc. Therefore, a considerable amount of research has been devoted to the control of flow separation. Corresponding to this effort, many possibilities to achieve separation control have been identified and thoroughly investigated. Among the most popular are shaping as a passive means and suction, blowing and wall movement as active control methods. Extensive reviews of the earlier research can be found in [8], the more recent literature is reviewed in [3] and [5], where the latter paper concentrates on the use of periodic excitation.

If the fluid in question is electrically conductive, the possibility arises that an electromagnetic body force may be used to influence the flow. This possibility has long been realized, especially in the field of liquid metals and other highly conductive materials like semiconductor melts. However, the application of Lorentz forces to fluids of small conductivity as sea water or other ionic media is less common, though first suggestions in the field of magneto-aerodynamics date back to the 1950s, e.g. [14]. Experimental evidence of successful separation postponement on a half cylinder in an electrolyte flow has been given

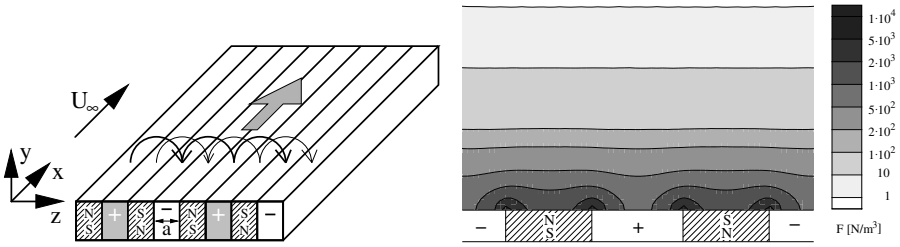

Figure 1. Configuration of electrodes and permanent magnets to generate a wall–parallel Lorentz force in streamwise direction (left) and force distribution in the y–z–plane (right).

by [2] in 1962. A renewed interest in the use of electromagnetic forces to control the flow of electrolytes arose in the 1990s. The main body of the corresponding research, among several others [11, 6, 1], dealt with the control of turbulent boundary layers for drag reduction. Separation prevention played only a tangential role. The aim of the present paper is to contribute some experimental results to this somewhat unattended topic, while concentrating on hydrofoils and scaling issues. Successful electromagnetic control of the flow around a circular cylinder at low Reynolds numbers has already been demonstrated in [21]. This generic problem was treated recently by a number of researchers, e.g. [7] and [13].

2. Principle and Parameters

An electromagnetic body force or Lorentz force $\mathbf{F}$ results from the vector product of the current density $\mathbf{j}$ and the magnetic induction $\mathbf{B}$

$$\mathbf{F} = \mathbf{j} \times \mathbf{B}. \tag{1}$$

The current density itself is given by Ohm's law:

$$\mathbf{j} = \sigma(\mathbf{E} + \mathbf{u} \times \mathbf{B}), \tag{2}$$

where $\mathbf{E}$ denotes the electric field, $\mathbf{u}$ the velocity, and σ the electrical conductivity, respectively. Since typical electrolytes have small conductivities in the order of $10\,\mathrm{S/m}$, the currents originating from the $(\mathbf{u} \times \mathbf{B})$–term in equation (2) are generally very low, even for magnetic fields of several tesla. As a consequence, the Lorentz force (1) due to these currents is almost undetectable. In order to obtain current densities large enough for flow control purposes it is therefore necessary to apply an electric field of magnitude E_0 with $E_0/(U_\infty B_0) \gg 1$, where B_0 denotes the applied magnetic field and U_∞ the velocity of the outer

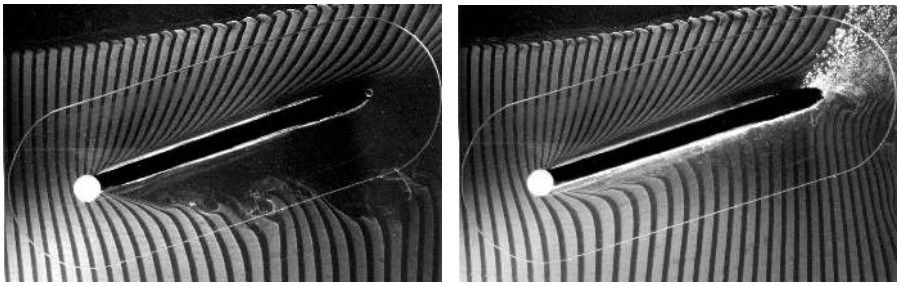

Figure 2. Inclined plate without (left) and with (right) suction side Lorentz force.

flow. This implies that the force density distribution can be determined independently of the flow field.

A wall parallel Lorentz force can be generated by a stripwise arrangement of flush mounted electrodes and permanent magnets as sketched in Figure 1. Such a device has been proposed by [4] as a means to prevent boundary layer transition. Similar configurations are given in [15] and [10], the latter patent claiming among other things the use for separation suppression and lift increase. The calculated force density distribution in the y–z–plane belonging to such a device is shown in the right subfigure of Figure 1. Apart from end effects, both electric and magnetic fields have only components in wall normal (y) and spanwise (z) direction. Consequently (see equation (1)), the Lorentz force possesses only a streamwise (x) component. Near the plate surface, strong spanwise variations of the force density are to be seen. Averaging over z, the mean force density shows an exponential decay with increasing wall distance and can be written as

$$F = \frac{\pi}{8} j_0 M_0 e^{-\frac{\pi}{a}y}, \tag{3}$$

with M_0 denoting the magnetization of the permanent magnets and j_0 the applied current density σE_0, respectively. The magnetic induction B_0 at the surface of the magnetic poles can be calculated from the geometry of the magnets and their magnetization M_0. Electrodes and magnets have the same width a.

The electromagnetic force density acts as a momentum source for the near wall flow. Its accelerating effect on the velocity distribution of a flat plate boundary layer has been experimentally verified by LDA measurements in [6] and [23]. Depending on the force strength, even a distinct wall jet can be established. Such a strong impact seems to be predestined for separation control. Figure 2 shows an 18°inclined flat plate at a chord length Reynolds number of $1.2 \cdot 10^4$ [22]. The left hand image gives the uncontrolled flow which separates at the leading edge, visualized by the hydrogen bubble method. A flat plate stalls already

at approximately 5°at such a low Reynolds number [16]. Applying a streamwise Lorentz force at the suction side, separation might be suppressed completely as can be seen on the right hand image. The larger bubbles raising from the trailing edge are due to the electrolytic reactions at the electrode surfaces, which are concomitant phenomena of the current feed thru the electrolyte.

Two parameters are commonly used in magnetohydrodynamics to characterize the strength of the Lorentz force. The interaction parameter

$$N = \frac{j_0 B_0 c}{\rho U_\infty^2} \tag{4}$$

describes the ratio of electromagnetic to inertial forces. Using the viscous forces as a base, one obtains the Hartmann number

$$Z = \frac{1}{8\pi} \frac{j_0 M_0 a^2}{\rho U_\infty \nu}, \tag{5}$$

here given in a slightly modified formulation following the approach of [20]. Relevant fluid properties are the density ρ and the kinematic viscosity ν. The characteristic length of both parameters differ, N is formed with the chord length c and Z with the electrode width a, respectively. While Z is derived from the flat plate boundary layer equations, the interaction parameter N comes from the normalization of the full Navier–Stokes equations. In analogy to the terminology used in separation control by blowing [12], one may also define an electro–magneto–hydrodynamic (EMHD) momentum coefficient:

$$C_{\mu EMHD} = \frac{1}{4} \cdot \frac{a j_0 M_0}{\rho U_\infty^2} \cdot \frac{x_e - x_s}{c}. \tag{6}$$

Here $x_e - x_s$ denotes the fraction of the chord covered with electrodes and magnets (see Figure 3). $C_{\mu EMHD}$ links the total momentum injected into the flow by the Lorentz force to the dynamic pressure. If the electrodes and magnets extend over almost the whole suction side of the foil, the interaction parameter may be converted to the EMHD momentum coefficient in reasonable approximation as

$$C_{\mu EMHD} \approx \frac{a}{2c} N. \tag{7}$$

As well interaction parameter and modified Hartmann number are not independent, since $Z/N \propto Re$.

However, a crucial point to assess the feasibility of electromagnetic separation control is the identification of an appropriate parameter describing the control mechanism. From a practical point of view, the

	PTL IV_L	PTL IV_S	NACA 0015
c[mm]	158	158	667
s[mm]	360	345	1088
s/c	2.28	2.18	1.63
a[mm]	10	5	10
a/c	0.06	0.03	0.015
x_s[mm]	12	6	25
x_e[mm]	131	134	563
B_0[T]	0.4	0.2	0.58
I_{max}[A]	50	50	1000
$Re_{max}/10^5$	1.2	1.2	3.7

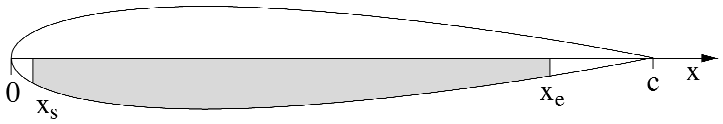

Figure 3. Parameters of the hydrofoils (left), the NACA 0015 before mounting to the force balance (right).

main issue is the scaling with the flow velocity, $Z \propto U_\infty^{-1}$ while N and $C_{\mu EMHD}$ are proportional to U_∞^{-2}.

3. Experimental Apparatus

Force measurements on three different symmetric hydrofoils have been performed in the "Arctic Environmental Test Basin" of the Hamburg Ship Model Basin (HSVA). A sodium chlorine solution with a conductivity equal to that of typical seawater ($\sim 3.5\,\mathrm{S/m}$) has been used for the experiments. The table inserted in Figure 3 gives the main dimensions of the foils. The shape of a PTL IV is similar to a NACA 0017 regarding the hydrofoil thickness in percent of the chord. However, the thickness distribution is slightly different. Mainly the leading edge radius is smaller for the PTL IV, whereas the slope in the trailing part is a little larger then in the case of the NACA 0017. The two PTL IV hydrofoils differ in their electromagnetic system. The electrode distance a of the PTL IV_L is 10 mm, that of the PTL IV_S 5 mm. As a consequence

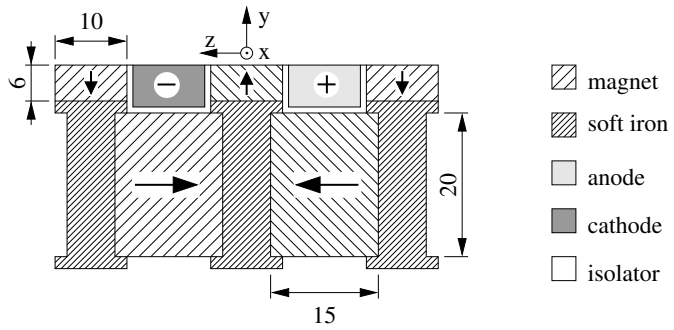

Figure 4. Cutaway sketch of the system of magnets and electrodes used at the NACA 0015. The magnetization direction of the magnets is denoted by arrows.

the penetration depth of the electromagnetic force into the flow differ on both foils, since it is completely determined by a (see equation (3)). Another difference among both foils is the electrode material: stainless steel for the PTL IV_L and titanium covered by RuO_2/IrO_2 for the PTL IV_S. The consequences of the chosen material on the flow might be larger than expected, since due to the chlorine evolution the stainless steel corrodes rapidly at the anodes. This corrosion leads to grooves on the foil surface. These corrosion effects are completely suppressed at the PTL IV_S, the mentioned material is known for its use in dimensionally stable anodes (DSA) [19]. The third foil, a NACA 0015 shown on the right hand side of Figure 3, has more than 4 times the chord length of the two PTL IV, allowing larger Reynolds numbers at equal speed. To maintain an aspect ratio larger one, also the span width s had to be increased in comparison with the PTL IV. A maximum current of $I_{max} = 1000\,\mathrm{A}$ can be fed to the stainless steel electrodes of the NACA 0015.

A sectional drawing of the electrode/magnet–system of the NACA 0015 is shown in Figure 4. Between two Nd–Fe–B permanent magnets which face each other with equal poles, a soft H–iron is mounted, concentrating the magnetic flux. On top of the H–iron, additional smaller magnets are glued to further increase the magnetic induction on the surface. The stainless steel electrodes are fixated between the small magnets. Each electrode is electrically isolated. In the case of the PTL IV_L, the small magnets on top of the H–irons are omitted and the electrodes are lowered accordingly in order to form a flat surface. Also, the dimensions of the base structure are scaled down to meet the construction requirements of the smaller foil. The PTL IV_S has the simplest arrangement of magnets and electrodes. It consists in the straightforward realization of the structure shown in Figure 1.

The "Arctic Environmental Test Basin" is an open channel 30 m long and 1 m deep. Four propellers drive the flow up to a maximum speed of approximately 1 m/s. For the measurements with the PTL IV hydrofoils, the width of the test section was reduced from 3 m to 0.8 m by a contraction. Both PTL IV foils have been vertically submersed in the test section and where equipped with endplates for the measurements. To avoid excessive blockage effects due to the large chord length of the NACA 0015, the contraction was not in place during the corresponding measurements. As a consequence, the free stream turbulence level at $U_\infty = 0.5$ m/s increased from about 0.5% to 3.5%. The NACA 0015 extended over the whole height of the channel, piercing the water surface. At the bottom, a gap of 6 mm remained. Forces have been measured on the PTL IV foils by a Kempf & Remmers rudder balance. The NACA 0015 had to be mounted on a larger balance of HSVA's own construction due to its weight of 172 kg. Signals of drag, lift and pitching moment were recorded at 10 Hz by a standard PC with a Hottinger Baldwin ADC Spider 8. The force values used in the following are time averages over time intervals of 20 s in the case of the two PTL IV and 80 s for the NACA 0015. Dynamic lift and drag variations caused by changing the angle of attack have been excluded from the averaging process. No corrections of any kind have been applied.

4. Results and Discussion

In the following, the usual definitions of lift and drag coefficient,

$$C_L = \frac{F_L}{\frac{\rho}{2} U_\infty^2 cs} \quad \text{and} \quad C_D = \frac{F_D}{\frac{\rho}{2} U_\infty^2 cs} \tag{8}$$

will be used. Here F_L denotes the lift and F_D the drag force, respectively. Due to reasons given later, the Lorentz force is characterized by the EMHD momentum coefficient in the next subsections.

4.1. Fixed angle of attack

At zero inclination angle α, the lift of a symmetric hydrofoil should be equal to zero. On a sufficiently slender foil, no separation would be expected. Figure 5 shows the effect of a single-side Lorentz force on lift and drag. A straight line of

$$C_D = 0.0239 - 1.01 \cdot C_{\mu EMHD} \tag{9}$$

can be fitted to the measured values of the drag coefficient. The slope of the linear relation equals almost exactly to minus one. That is,

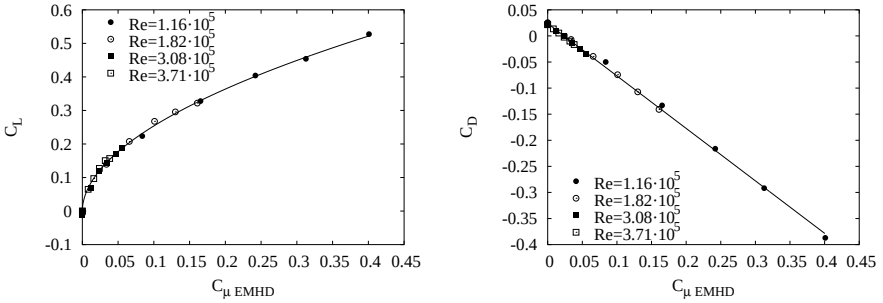

Figure 5. Lift and drag coefficient for the NACA 0015 in parallel flow ($\alpha = 0°$) versus $C_{\mu EMHD}$, different Reynolds numbers.

the thrust generated by the Lorentz force drives the hydrofoil very efficiently. In fact, the efficiency is even a little larger than one, which should be attributed to an underestimation of the Lorentz force actually applied. Since the initial drag of the foil is low, the total drag of the hydrofoil is negative for most $C_{\mu EMHD}$ values.

Due to the asymmetric acceleration a lift force develops with increasing momentum coefficient, circulation is generated. The measured C_L values may be described by the following fit

$$C_L = 0.843 \cdot C_{\mu EMHD}^{0.521}. \tag{10}$$

Hence, as shown in the left part of Figure 5, a scaling as approximately $C_L \sim \sqrt{C_{\mu EMHD}}$ has been found. This would indicate a similar behavior as found in the case of circulation control by blowing [18].

Figure 6 gives drag and lift values for the NACA 0015 at 18°of attack. The flow is attached except for $C_{\mu EMHD} = 0$ and the two lower Reynolds numbers of $Re = 1.15 \cdot 10^5$ and $Re = 1.82 \cdot 10^5$. As in the case of the hydrofoil in parallel flow, the drag coefficients depend linearly on the EMHD momentum coefficient with the aforementioned exceptions. Disregarding these values, a straight line fit results in

$$C_D = 0.229 - 1.07 \cdot C_{\mu EMHD}. \tag{11}$$

Again, the slope of this line equals to one in good approximation. The proportionality of the lift coefficient and the square root of the momentum coefficient can be detected likewise:

$$C_L = 1.02 + 2.26 \cdot C_{\mu EMHD}^{0.478}. \tag{12}$$

Since the inclination angle is relatively high, both the initial lift coefficient and the coefficient are larger than those for $\alpha = 0°$. While the first is evident, the latter is similar to the findings in circulation control by blowing.

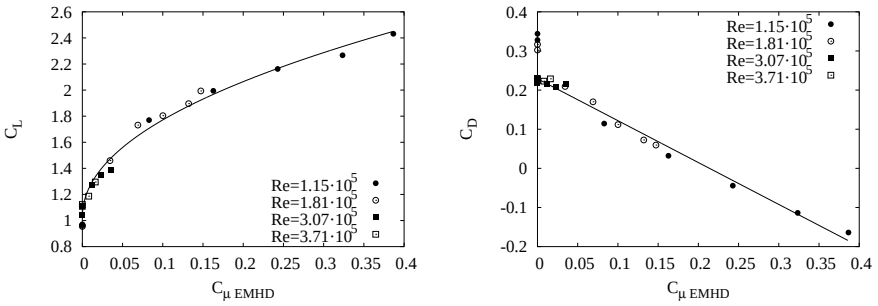

Figure 6. Lift and drag coefficient for the NACA 0015 at $\alpha = 18^\circ$ versus $C_{\mu EMHD}$, different Reynolds numbers.

At lower Reynolds numbers, a 17°inclined PTL $\mathrm{IV_L}$ is already stalled. The left part of Figure 7 shows the lift increment with increasing EMHD momentum coefficient. In comparison to the graphs in Figures 5 and 6 the dependency is more complex. At small momentum coefficients, the lift increase is steep, while it flattens for higher $C_{\mu EMHD}$. It may be helpful to compare the findings again with results from separation control by blowing. On the right hand side of Figure 7, ΔC_L versus C_μ values for blowing over a flap are given according to [17, 12]. Schwier [17] used a NACA 23015 in parallel flow with a 45°deflected flap. A jet was blown from a slit over the flap shoulder. Poisson–Quinton [12] rearranged Schwiers measurements using the momentum coefficient as a parameter for the blowing intensity. This collapsed Schwiers values fairly well. Two different regimes can be identified, boundary layer control (BLC) for small values of the momentum coefficient and circulation control for large C_μ. The corresponding parts of the figure are gray shaded. In the boundary layer control regime, a gradual reattachement of the separated flow over the flap takes place. This leads to a comparatively large increase of the lift coefficient. The momentum coefficient corresponding to complete reattachement $C_{\mu r}$ marks the upper end of the boundary layer control regime. At $C_\mu > C_{\mu r}$ the lift gain is smaller and proportional to $\sqrt{C_\mu}$, circulation control dominates the physics of the flow.

It would appear that the same classification may be applied to the left hand side of Figure 7 showing electromagnetic separation control. Even the numerical values of ΔC_L and $C_{\mu r}$ match surprisingly well, though this should be attributed to pure chance, since the flow conditions are quite different in both cases. However, the general trends are obviously the same.

While mean values of the lift coefficient are given in Figure 7, Figure 8 reveals the instationary nature of the reattachement process showing

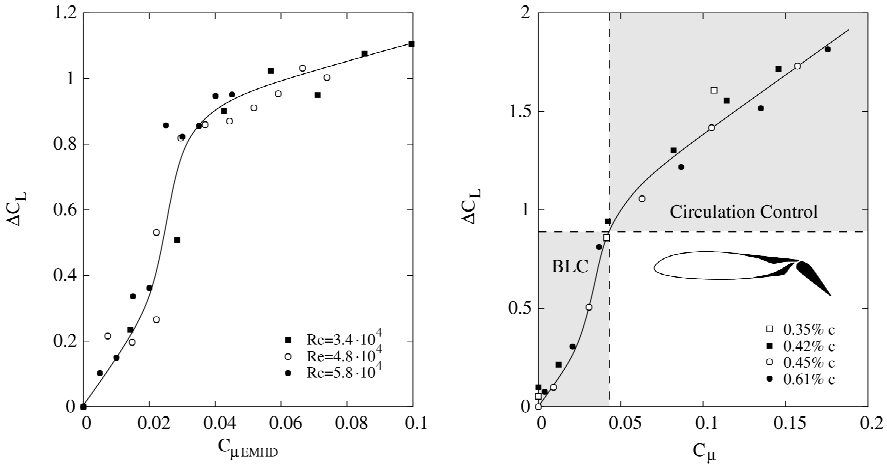

Figure 7. ΔC_L versus $C_{\mu EMHD}$ for the PTL $\mathrm{IV_L}$ at $\alpha = 17°$ (left). Blowing over a 45°inclined flap on a NACA 23015, measured values from [17] according to [12] with the blowing slot width as a parameter (right).

the 10 Hz sampled time signal of lift and momentum coefficient for the 16°inclined PTL $\mathrm{IV_S}$ at a Reynolds number of $Re = 5.7 \cdot 10^4$. At small values of the EMHD momentum coefficient, the lift increases steadily. From $C_{\mu EMHD} \approx 0.0056$ onwards, the lift coefficient oscillates between two values, which might be assigned on the one hand to a separated and on the other hand to a reattached flow. The erratic lift increment is about twice as large as the former increase due to $C_{\mu EMHD} \approx 0.0056$. This regime of large amplitude oscillations merges into a stable state for $C_{\mu EMHD} \gtrapprox 0.0084$. A further increase of the injected momentum results only in weak lift increases, the circulation control regime is reached. $C_{\mu r}$ is noticeable smaller than for the PTL

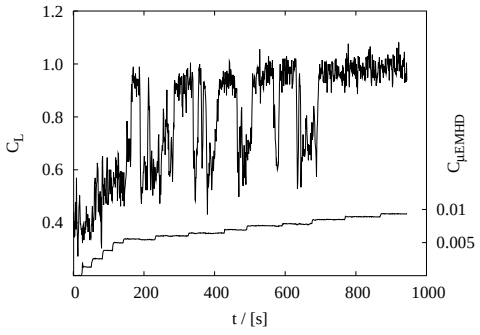

Figure 8. C_L and $C_{\mu EMHD}$ for the PTL $\mathrm{IV_S}$ at $\alpha = 16°$ and $Re = 5.7 \cdot 10^4$ versus time.

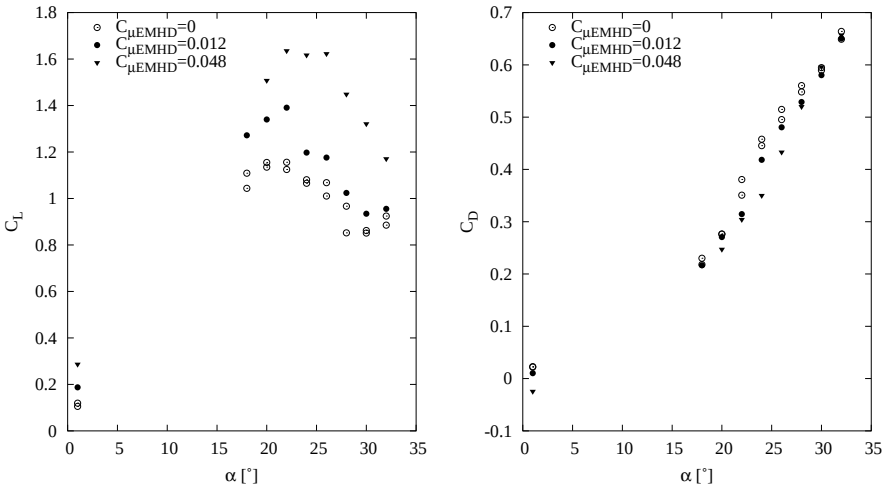

Figure 9. Lift and drag coefficient for the NACA 0015 versus angle of attack at $Re = 3.0 \cdot 10^5$.

$\mathrm{IV_L}$, although the angle of attack corresponding to the Figures 7 and 8 differ only slightly. In fact, due to the corrosion problematic described above, both hydrofoils may be much less similar then expected.

4.2. Lift and drag versus angle of attack

Both effects, separation and circulation control, are evident also in the C_L versus α and C_D–α curves shown in Figure 9. Only points at $\alpha = 1^\circ$ and around the stalling angle have been measured for the NACA 0015. As already shown, at small angles of attack, the suction side Lorentz force increases lift and decreases drag, the corresponding measurement points are shifted accordingly. At higher angles of attack, separation prevention gains importance. Due to the Lorentz force acting as a source of momentum for the near wall flow, stalling takes place at higher angles of attack then in the unforced case. Therefore, a higher maximum lift corresponding to the higher maximum angle of attack can be established. Obviously, also the type of stall is influenced by the suction side Lorentz force. While the loss of lift is relatively moderate for the unforced NACA 0015, it is larger and abrupt for the forced hydrofoil. The drag of the forced foil is always smaller than that of the unforced, most pronounced when the unforced flow is separated while the forced flow remains attached.

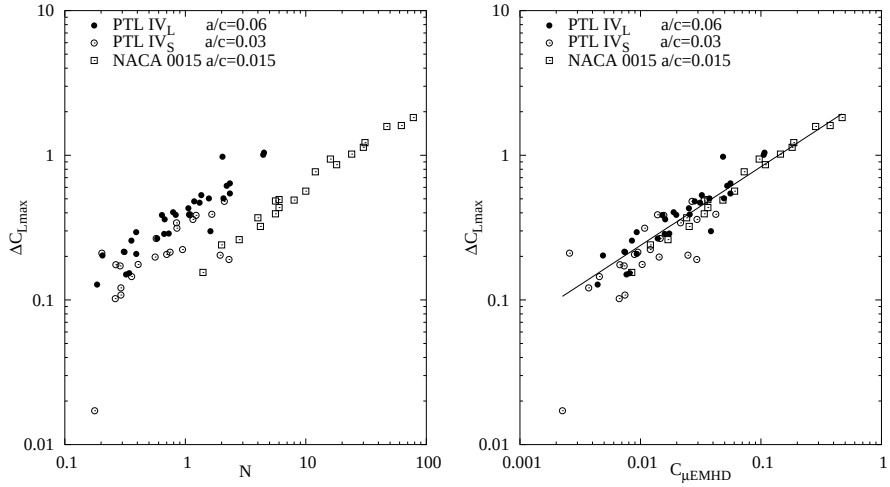

Figure 10. Scaling of ΔC_{Lmax} with the interaction parameter (left) and the EMHD momentum coefficient (right) in the Reynolds number range $2.9{\cdot}10^4 \leq Re \leq 3.7{\cdot}10^5$.

4.3. Scaling of the maximum lift gain

From a practical point of view, the maximum attainable lift gain ΔC_{Lmax} corresponding to a certain EMHD momentum coefficient is of considerable interest. This quantity may be written as

$$\Delta C_{Lmax}(C_{\mu EMHD}) = C_{Lmax}(C_{\mu EMHD}) - C_{Lmax}(C_{\mu EMHD} = 0). \quad (13)$$

Similar definitions could be written with the interaction parameter or the Hartmann number instead of $C_{\mu EMHD}$. Since it is influenced by several physical mechanisms and flow conditions, ΔC_{Lmax} might not be well suited to gain better insight into the flow physics. However, it enables a reasonable evaluation of the benefits achievable with the control approach.

Figure 10 shows on a log–log scale the maximum lift gain on the left versus the interaction parameter and on the right versus the EMHD momentum coefficient. A corresponding figure with the Hartmann number as parameter describing the Lorentz force has been omitted, since no correlation could be detected. The figures compile data points of all three hydrofoils in the Reynolds number range $2.9{\cdot}10^4 \leq Re \leq 3.7{\cdot}10^5$ and corresponding to measurements with and without tripping devices. A certain scatter is therefore unavoidable, especially since the Reynolds number range in question is very widely known for its diversity of flow phenomena on airfoils [9].

In the figure showing ΔC_L versus N, the points belonging to one hydrofoil form distinct lines. The effect of the interaction parameter

defined with the chord as characteristic length is specific to each foil. It appears that the larger the relative penetration depth a/c of the force into the fluid, the higher the maximum momentum gain. Since the EMHD momentum coefficient accounts for the integral force, it includes the effect of the varying penetration depth (see equation (7)) and collapses most points sufficiently well. A simple power law fit results in

$$\Delta C_L = 2.91 \cdot C_{\mu EMHD}^{0.544}. \tag{14}$$

The superscript of $C_{\mu EMHD}$ is very near to 0.5, suggesting that circulation control plays an important role in the parameter range investigated.

4.4. Conclusions

The influence of a wall parallel streamwise Lorentz force on the flow around hydrofoils has been studied in a saltwater flow. As could be expected, separation as well as circulation can be readily controlled by such a force configuration. The effect of the force on the flow is very similar to that reported for flow control by blowing. Indeed, the definition of an electro–magneto–hydrodynamic momentum coefficient allows a direct comparison of both control methods.

If the Lorentz force acts on an already attached flow, the resulting lift increase is proportional to the square root of the momentum coefficient. The lift gain is more pronounced, if the Lorentz force leads to a reattachement of an otherwise separated suction side flow. A time resolved view on the reattachement process reveals that this flow is intermittent for a certain range of the EMHD momentum coefficient.

The maximum attainable lift gain under different flow conditions and Reynolds numbers may as well be described by the momentum coefficient. This allows a first assessment of the relevance of electromagnetic separation control to practical applications.

Acknowledgements

Financial support from VDI under Grant NLD–FKZ 13N7134/1 and DFG under Grant INK 18/A1–1 is gratefully acknowledged.

References

1. Du, Y., Karniadakis, G. Em., Suppressing wall turbulence by means of a transverse traveling wave. *Science* **288** (2000) 1230–1234.

2. Dukure, R., Lielausis, O., Experimental investigation of the effect of electromagnetical forces upon flow around bodies in electrolyte. In: *Problems of Magnetohydrodynamics and Plasmadynamics* (Voprosi Magnitnoi Gidrodinamiki i Dinamiki Plazmi), Riga (1962) 647–650.
3. Gad–el–Hak, M., Bushnell, D. M., Separation Control: Review. *J. Fluids. Engng.* **113** (1991) 5–30.
4. Gailitis, A., Lielausis, O., On a possibility to reduce the hydrodynamical resistance of a plate in an electrolyte, *Applied Magnetohydrodynamics. Reports of the Physics Institute*, **12** (1961) 143–146 (in Russian).
5. Greenblatt, D., Wygnanski, I. J., The control of flow separation by periodic excitation. *Prog. Aero. Sci.* **36** (2000) 487–545.
6. Henoch, C., Stace, J., Experimental investigation of a salt water turbulent boundary layer modified by an applied streamwise magnetohydrodynamic body force. *Phys. Fluids* **7** (1995) 1371–1383.
7. Kim, S.–J., Lee, C. M., Investigation of the flow around a circular cylinder under the influence of an electromagnetic force. *Exp. Fluids* **28** (2000) 252–260.
8. Lachmann, G. V., Boundary Layer and Flow Control, **2**, Pergamon Press, (1961).
9. Lissaman, P. B. S., Low–Reynolds–Number Airfoils. *Ann. Rev. Fluid Mech.* **15** (1983) 223–239.
10. Meyer, R. X., Magnetohydrodynamic method and apparatus. US Patent 3,360,220 (1967).
11. Nosenchuck, D. M., Brown, G. L., Discrete spatial Control of wall shear stress in a turbulent boundary layer. In: *Near–Wall Turbulent Flows*, Eds. R. M. C. So, C. G. Speziale, B. E. Launder, Publisher Elsevier (1993) 689–698.
12. Poisson–Quinton, P. H., Einige physikalische Betrachtungen über das Ausblasen an Tragflügeln. *Jahrbuch der WGL* (1956) 29–51.
13. Posdziech, O., Grundmann, R., Electromagnetic control of seawater flow around circular cylinders. *Europ. J. Mechanics/B Fluids* **20** (2001) 255–274.
14. Resler, E. L., Jr., Sears, W. R., The Prospects for Magneto–Aerodynamics. *J. Aero. Sci.* **25** (4) (1958) 235–245.
15. Rice, W. A., Propulsion system. US Patent 2,997,013 (1961).
16. Schmitz, F. W., Aerodynamik des Flugmodells. Tragflügelmessungen I. C.J.E. Volckmann Nachf. E. Wette, Berlin–Charlottenburg (1942).
17. Schwier, W., Blasversuche zur Auftriebssteigerung am Profil 23015 mit verschiedenen Klappenformen. *Technical Report* FN 1865, Zentrale f. wiss. Berichtswesen, Berlin–Adlershof (1943).
18. Siestrunck, R., General theory of the jet flap in two–dimensional flow. In: [8].
19. Trasatti, S., Physical Chemistry of ceramic oxides. *Electrochimica Acta* **36** (2) (1991) 225–241.
20. Tsinober, A. B., Shtern, A. G, On the possibility to increase the stability of the flow in the boundary layer by means of crossed electric and magnetic fields. *Magnitnaya Gidrodinamika* **3** (2) (1967) 152–154 (in Russian).
21. Weier, T., Gerbeth, G., Mutschke, G., Platacis, E., Lielausis, O., Experiments on cylinder wake stabilization in an electrolyte solution by means of electromagnetic forces localized on the cylinder surface. *Experimental Thermal and Fluid Science* **16** (1998) 84–91.
22. Weier, T., Fey, U., Gerbeth, G., Mutschke, G., Avilov, V., Boundary layer control by means of electromagnetic forces. *ERCOFTAC Bulletin* **44** (2000) 36–40.

23. Weier, T., Fey, U., Gerbeth, G., Mutschke, G., Lielausis, O., Platacis, E., Boundary layer control by means of wall parallel Lorentz forces. *Magnetohydrodynamics* **37** (1/2) (2001) 177-186.